# PLANNING SENSORLESS ROBOT MANIPULATION OF SLIDING OBJECTS

**M. A. Peshkin** and **A. C. Sanderson***
Robotics Institute
Carnegie-Mellon University
Pittsburgh, Pennsylvania 15213

**ABSTRACT:** The physics of motion of a sliding object can be used to plan sensorless robot manipulation strategies. Prediction of a sliding object's motion is difficult because the object's distribution of support on the surface, and the resulting frictional forces, are in general unknown. This paper describes a new approach to the analysis of sliding motion, which finds the set of object motions for *all* distributions of support. The analysis results in the definition of discrete regions of guaranteed sticking and slipping behavior which lend themselves to use in planning. Unlike previous work our approach produces quantitative bounds on the *rate* at which predicted motions can occur. To illustrate a manipulation plan which requires quantitative information for its construction, we consider a strategy based on "herding" a sliding disk toward a central goal by moving a robot finger in a decreasing spiral about the goal. The optimal spiral is constructed, and its performance discussed.

**KEYWORDS:** Center of rotation, sliding, slipping, pushing, grasping, manipulation, sensorless manipulation, friction, robot, planning.

This work was supported by a grant from Xerox Corporation, and by the Robotics Institute, Carnegie-Mellon University.

## 1. Introduction

Sliding operations can be used constructively to manipulate and acquire objects, without sensing, and despite uncertainty in the orientation and position of the object. For instance, in a typical grasping operation a robot opens a two-jaw gripper wide enough to accommodate both an object to be grasped, and any uncertainty in the object's position. In the general case, the object will be nearer initially to one jaw than to the other, and as the jaws close the nearer jaw will make contact first. There follows a sliding phase until the second jaw makes contact. During the sliding phase the object is likely to rotate. (Once both jaws come into contact with the object, sliding on the table becomes less important than *slipping* of the object with respect to the faces of the jaws. This regime will not be considered here.) The behavior of an object during both phases is discussed in [1]. Brost finds grasp strategies which bring the object into a unique configuration in the gripper, despite substantial uncertainty in its initial configuration.

* Current address: Philips Laboratories, Briarcliff Manor, NY

Another example of the use of sliding is the interaction of an object on a moving belt or ramp (as in a parts feeder) with a fixed, slanted, fence. (Equivalently the object may be on a stationary table, and the fence moving under robot control.) One of many possible behaviors of the object when it hits the fence is to rotate until a flat edge is flush against the fence, and then to slide along the fence. The behavior of objects on encountering a fence has been considered in [1] and [2]. In [2], Mani and Wilson find strategies for manipulation which can orient an object on a table by pushing it in various directions with a fence. Each push aligns a facet of the object with the fence.

R. P. Paul demonstrated a clever grasping sequence on a hinge plate. The strategy makes use of sliding to simultaneously reduce the uncertainty of a hinge plate's configuration to zero, and then to grasp it [3] [5]. To understand this and similar operations, Mason [3] determined the conditions required for translation, clockwise (CW) rotation, and counter-clockwise (CCW) rotation of a pushed object. Mason's results are used in both [1] and [2], and also in this work.

The contribution of our work, summarized in section 2, is to place quantitative bounds on the *rate* at which a predicted motion occurs, and to demonstrate the application of these bounds to the planning of manipulation tasks. Without rate information none of the above methods can produce manipulation strategies guaranteed to succeed. For instance, to implement one of Mani and Wilson's orientation strategies, it is necessary to find the worst case distance a sliding object must be pushed by a fence, before a flat edge of the object comes into alignment with the fence. The rate information found by our method can be used to determine the worst-case distance.

## 2. Summary of Analytical Results

A sliding object has three degrees of freedom. If we require the object to be in contact with another object (a pusher), the sliding object retains two degrees of freedom, which are most conveniently expressed as the coordinates of a point in the plane called the *center of rotation* (COR). Any infinitesimal motion of the object can be expressed as a rotation $\delta\theta$ about some COR, chosen so that the infinitesimal motion of each point $\vec{w}$ of the object is perpendicular to the vector from the COR to the point $\vec{w}$

Finding the COR of a sliding object in planar contact with a surface is complicated by the fact that changes in the distribution of support forces under the object substantially affect the motion. The distribution of support may be changed dramatically by tiny deviations from flatness of the surfaces. Since we wish to

determine the motion of any object, without knowing the distribution of support for it, our goal is to find the locus of CORs under *all* possible support distributions.

The coefficient of friction with the supporting surface ($\mu_s$) does not affect the motion of the object if we use a simple Coulomb model of friction. It is also assumed that all motions are slow (the *quasi-static approximation*. [4])

We will take the object being pushed to be a disk with its center of mass (CM) at the center. Given another object of interest (e.g. a square), we can consider a disk centered at the CM of the square, big enough to enclose it. The radius $a$ of the disk is the maximum distance from the CM of the square to any point on the square. Since any support distribution on the square could also be a support distribution on the disk, the COR locus of the disk must enclose the COR locus of the square. The locus for the disk therefore provides useful bounds on the locus for the real object.

The parameters of the COR problem are the point of contact $\vec{c}$ between the pusher and the object, and the angle $\alpha$ between the edge and the line of pushing, as shown in figure 2-1. The values of $\alpha$ and $\vec{c}$ shown are the ones which are needed in considering the motion of the five-sided object shown inscribed in the disk. We do not require the point of contact $\vec{c}$ to be on the perimeter of the disk, as this would eliminate applicability of the results to objects inscribed in the disk. Similarly, we do not require $\alpha$ to be such that the edge being pushed is perpendicular to vector $\vec{c}$, as it would be if the object were truly a disk. The disk (with radius $a$), $\alpha$, $\vec{c}$, and the CM, are shown in figure 2-1. A particularly simple distribution of support forces, in which the support is concentrated at just a "tripod" of points ($\vec{u}_1, \vec{u}_2, \vec{u}_3$) is indicated, along with what might be the COR for that distribution of support.

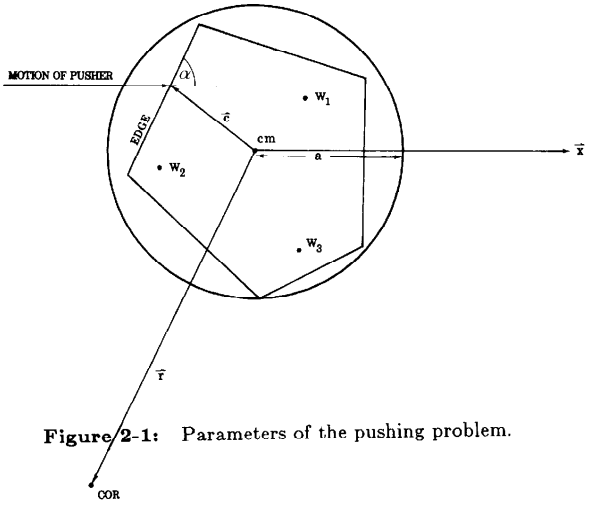


**Figure 2-1:** Parameters of the pushing problem.

Peshkin and Sanderson [6] analyze the motion of the sliding object in detail. The approach is to minimize the energy dissipated by friction with the surface for arbitrary infinitesimal motions. Analytical relations are found between the set of all support distributions, an intermediate formulation called the Q-locus, and the locus of CORs. Boundaries of the COR locus are found by evaluating the resulting analytical expressions.

Figure 2-2 shows examples of the COR loci found [6] for various values of $\alpha$ and $\vec{c}$. In each section the angle $\alpha$ of the edge with respect to the line of pushing is indicated. The edge may be the front edge of a fence pushing a corner of an inscribed object, or it may be an edge of the inscribed object in contact with a pushing point (as in figure 2-1). $\vec{c}$ is the vector from the CM (at the center of the disk) to the point of contact indicated by the arrowhead. The boundary of the COR locus is shown in bold outline. Every point within the locus is the COR for some possible distribution of support forces on the disk. Our results [6] indicate that no distribution of support forces can result in a COR outside the boundary shown. In figure 2-2, the coefficient of friction between the pusher and the object ($\mu_c$) is zero. These elementary COR loci are denoted $\{COR\}_\alpha$.

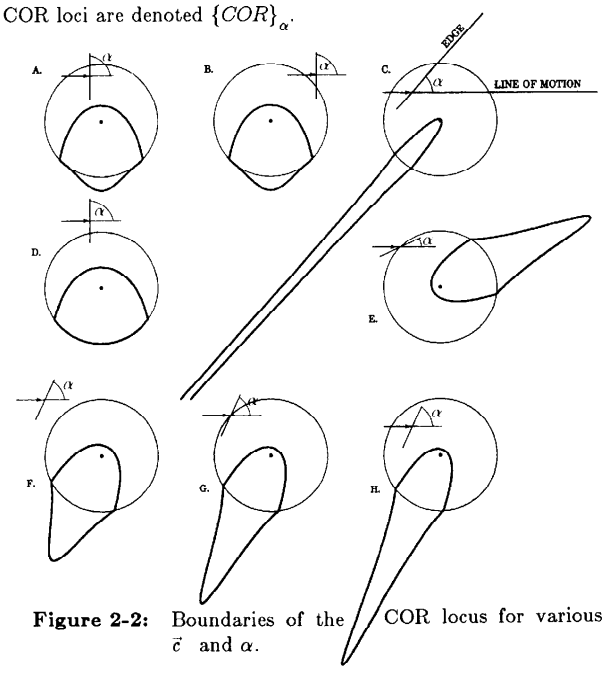


**Figure 2-2:** Boundaries of the COR locus for various $\vec{c}$ and $\alpha$.

Defining the unit vector $\vec{\alpha} = (\cos\alpha, \sin\alpha)$, we observe that the COR loci have an axis of symmetry about $\vec{\alpha}$. Note that the pushing force is directed perpendicular to $\vec{\alpha}$, (not parallel to the line of motion,) since $\mu_c = 0$. We see in figure 2-2(c), that if the pushing force is directed from the point of contact almost directly through the CM, the maximum distance from the CM to an element of the COR locus becomes great. This distance, called $r_{tip}$, is infinite if the pushing force is directed at the CM, as shown by Mason [3]. In [6] we found a simple formula for $r_{tip}$:

$$r_{tip} = \frac{a^2}{\vec{\alpha}\cdot\vec{c}} \qquad (1)$$

As the angle $\alpha$ is varied, the tip of $\{COR\}_\alpha$ traces out a straight line called the *tip line*. The tip line, (figure 2-3), is perpendicular to $\vec{c}$, and a distance $a^2/c$ from the CM.

If the coefficient of friction between pusher and object $\mu_c$ is non-zero, we find that we can combine two of the elementary ($\mu_c = 0$) COR loci (such as are shown in figure 2-2), and the tip line construction, to create a *COR sketch* comprising all the possible locations of the COR for the system with non-zero friction $\mu_c$. A COR sketch is shown in figure 2-4. The two elementary COR loci

$\{COR\}_{\alpha\pm\nu}$, which are to be combined, are shown in outline. The half-width of the friction cone is $\nu = \tan^{-1}\mu_c$. The locus of possible values of the COR consists of three distinct intersection regions: (1) the part of the elementary COR locus $\{COR\}_{\alpha+\nu}$ left of the sticking line (shown shaded), (2) the part of $\{COR\}_{\alpha-\nu}$ right of the sticking line (also shaded), and (3) part of the *sticking line* (described below) above the tip line.

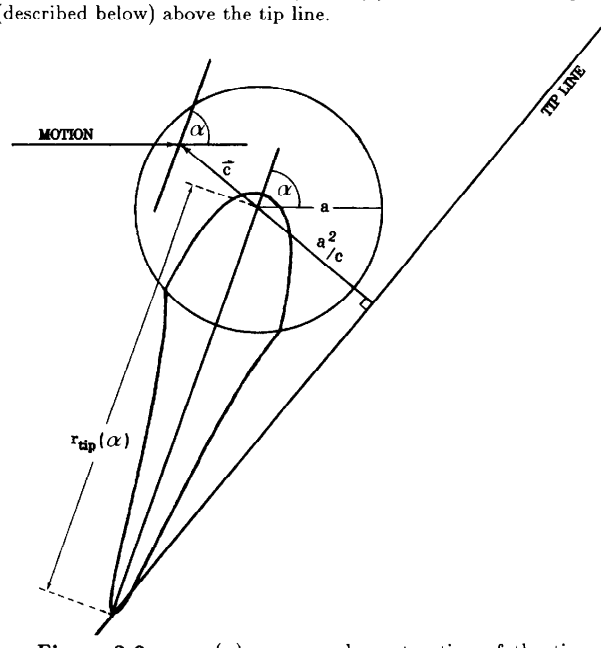


**Figure 2-3:** $r_{tip}(\alpha)$ vs. $\alpha$, and construction of the tip line.

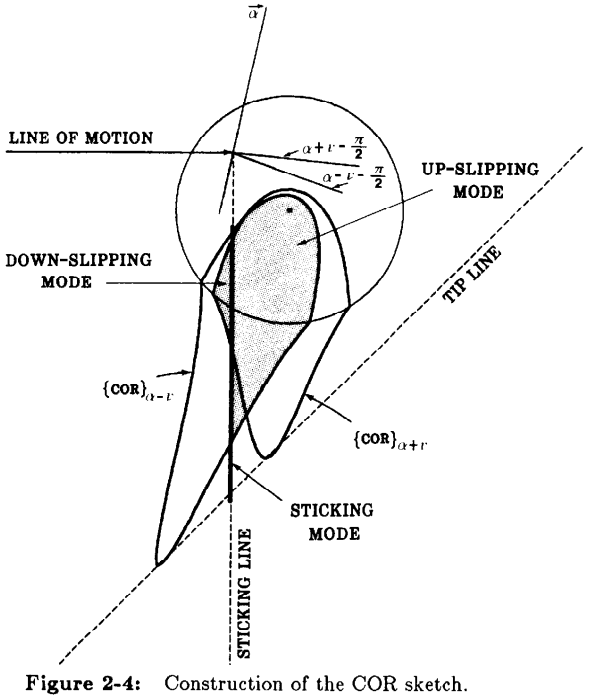


**Figure 2-4:** Construction of the COR sketch.

### 2.1. Modes of Motion

The *sticking line* is the normal to the line of motion of the pusher, at the point of contact. If the COR lies on the sticking line, there is no slipping of the object relative to the pusher as motion advances. If the COR lies left (resp. right) of the sticking line, the object slips down (resp. up) relative to the pusher as motion advances. The three component parts of the COR sketch described above are designated the *down-slipping, up-slipping,* and *sticking* loci, respectively. In the example shown, any of the three modes of motion (sticking, slipping down, slipping up) are possible, but this is not always the case. We can determine the possible modes of motion, and their minimum and maximum rates, by constructing the COR sketch [7].

Whether a clockwise or a counterclockwise mode of rotation occurs can also be determined from the COR sketch, or by using the rules found by Mason [3].

### 2.2. Application to Gross Motion

We have seen how bounds can be placed on the possible *instantaneous* motions of a sliding object being pushed by another object, in the presence of unknown frictional forces between object and table, and between object and pusher. Often we wish to calculate not the bounds on the instantaneous of motion, as above, but bounds on a gross motion of the object which can occur concurrently with some other gross motion of known magnitude. (For instance, we may wish to find bounds on the displacement of the pusher which occurs while the object rotates 15 degrees.) Our approach to dealing with gross motion follows a definite strategy outlined below, and explained in more detail in [7]. Examples are given in [7].

Suppose we wish to find the greatest possible change in a quantity $x$, while quantity $\beta$ changes from $\beta_{initial}$ to $\beta_{final}$. From the geometry of the problem we find a *differential equation of motion* relating the instantaneous motions $dx$ and $d\beta$. We then construct the COR sketch for each value of $\beta$. In each sketch we locate the possible COR which maximizes $dx/d\beta$. Using that COR, we integrate the differential equation of motion from $\beta_{initial}$ to $\beta_{final}$, yielding an upper bound for the quantity $x$.

## 3. Planning Sensorless Manipulation

Planning a sensorless manipulation strategy requires construction of a sequence of interactions of pusher with pushed object, such that the set of all possible positions of the object (which in our case is a subset of three dimensional configuration space) is reduced from an initial volume to a smaller final volume. Optimally the final set of configurations consists of just a point in configuration space. Manipulation with sensory feedback permits comparison of intermediate states with goal states in order to modify the control strategy. In sensorless manipulation prediction of intermediate states depends on reliable models of motion. The models are used to determine preconditions and results of each operation, and a plan evolves by matching a series of subgoals to bounds on motion in order to constrain resulting configurations.

For planning of manipulation strategies it is useful to have a graphical representation of the mode of motion of the sliding object (i.e. clockwise rotation, counterclockwise rotation, up-slipping, down-slipping, and sticking), as a function of the parameters which determine the mode: object orientation, and direction of pushing. Since in many cases more than one mode is possible, the regions corresponding to each mode may overlap.

Brost [1] and Mani [2] have independently developed graphical representations for a simplified set of modes of motion consisting of only clockwise and counterclockwise rotation. Using our results the representations can be extended to incorporate the slipping and sticking modes.

Design of manipulation strategies requires, first, that the possible modes of motion be understood. This understanding can be used to guide a search for pusher motions which reduce the configuration space volume of the possible positions of the pushed object. But using only the set of modes, it is not possible to produce a guaranteed manipulation strategy. It is also necessary to understand the *quantitative* response of the pushed object to any proposed push. Since in general one must consider the effect of a proposed push on every possible initial position of the pushed object, it is essential that calculating the effect of a push be computationally inexpensive.

The qualitative and quantitative results described in section 2 fulfill both of the requirements listed above.

# 4. Spiral Localization of a Disk

Several examples of sensorless manipulation strategies are analyzed in [6] and [7], using the results summarized above (section 2). In this section we describe an unusual robot motion by which a disk, free to slide on a tabletop, can be localized without sensing. The approach is to enclose the set of possible initial position of the disk within a spiral executed by a robot finger. As the spiral decreases in radius, the disk is to be pushed towards the center of the spiral. Our quantitative results allow us to optimize this strategy by choosing the maximum convergence rate of the spiral subject to the constraint that the object must not escape.

If the disk is known initially to be located in some bounded area of radius $b_1$, we begin by moving a point-like pusher in a circle of radius $b_1$. Then we reduce the pusher's radius of turning by an amount $\Delta b$ with each revolution, so that the pusher's motion describes a spiral. Eventually the spiral will intersect the disk (of radius $a$), bumping it. We wish the disk to be bumped toward the center of the spiral, so that it will be bumped again on the pusher's next revolution. If the spiral is shrinking too fast, however, the disk may be bumped *out* of the spiral instead of toward its center, and so the disk will be lost and not localized.

We wish to find the maximum shrinkage $\Delta b$ consistent with guaranteeing that the disk is bumped into the spiral, and not out. ($\Delta b$ will be a function of the present spiral radius.) We also wish to find the number of revolutions which will be required to localize the disk to some radius $b$, with $a < b < b_1$, and the limiting value of $b$, called $b_\infty$, below which it will not be possible to guarantee localization, regardless of the number of revolutions.

### 4.1. Analysis

Suppose the pushing point has just made contact with the disk. Since the previous revolution had radius only $\Delta b$ greater than the current revolution, the pusher must contact the disk at a distance at most $\Delta b$ from the edge of the disk, as shown in figure 4-1. We will consider only the worst case, where the distance of the pusher from the edge is the full $\Delta b$.

We know that if $\Delta b < a$ the disk will move downward [3]. This is not sufficient to assure that the disk will be pushed into the spiral (rather than out of the spiral), because the pushing point will also move down, as it continues along its path (figure 4-1). To guarantee that the disk will be pushed into the spiral, we must make sure that it moves down *faster* than does the pushing point.

One way of comparing rates of moving down is by considering the increase or decrease in the angle $\beta$, called the *collision parameter*, in figure 4-1. If as the pusher's motion along its spiral progresses $\beta$ increases, the disk is being pushed *into* the spiral; localization is succeeding. But if as the pusher's motion progresses $\beta$ decreases, the disk is being pushed *out* of the spiral; localization is failing.

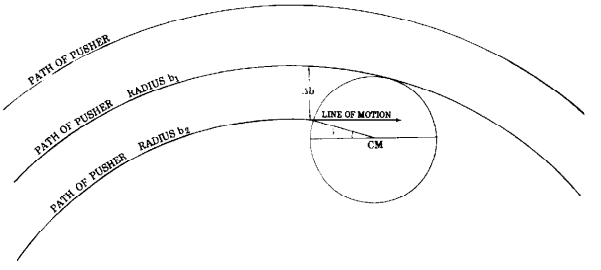


**Figure 4-1:** Geometry at the moment of the second collision of pusher and disk.

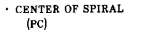


### 4.2. Critical Case: Pusher Chasing the Disk around a Circular Path

In the critical case the angle $\beta$ does not change with advance of the pusher. The critical case, shown in figure 4-2, is unstable. The pusher's motion is shown as an arc of a circle, labeled *path of pusher*, and centered at *PC*. To maintain the critical case, the path followed by the CM of the disk (labeled *critical path of CM*) must be as shown in the figure: an arc of a circle, concentric with the arc *path of pusher*. Instantaneously, the direction of motion of the CM must be along the line labeled *motion of CM*, tangent to the *critical path of CM*. The *critical line*, drawn through *PC* and *CM*, is by construction perpendicular to the line *motion of CM*. The COR of the disk must fall on the *critical line*, in order that the instantaneous motion along the line *motion of CM* be tangent to the *critical path of CM*.

If the COR falls to the left of the *critical line*, the CM diverges from the *critical path of CM* by moving *inside* the arc. Therefore $\beta$ will increase with advance of the pusher (i.e. localization is succeeding.) If the COR falls to the right of the *critical line*, the CM diverges from the *critical path of CM* by moving *outside* the arc. Therefore $\beta$ will decrease with advance of the pusher (i.e. localization is failing.) The *critical line* divides the plane into two zones: if the COR falls in the left zone, the disk is pushed into the pusher circle, while if the COR falls in the right zone, the disk is pushed out of the pusher circle.

In figure 4-3 we have constructed the COR sketch with collision parameter $\beta$. To make sure that the whole COR locus falls to the left of the *critical line*, we need only place the center of the pusher motion (*PC*) *below* the lower endpoint of the sticking locus. The figure shows the marginal case where *PC* is exactly at the lower endpoint of the sticking locus.

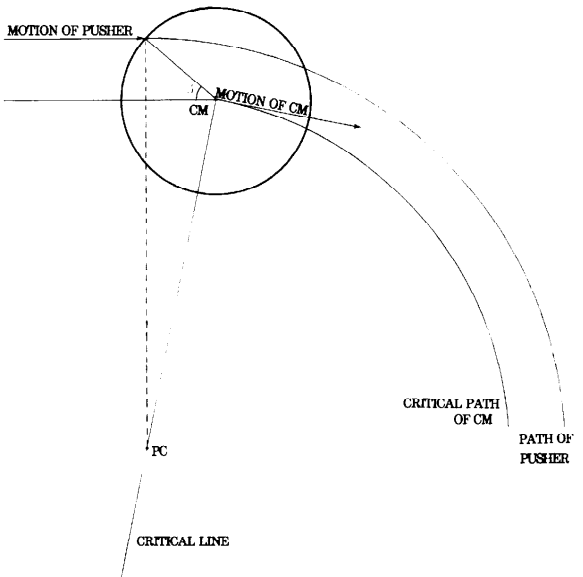


**Figure 4-2:** Critical case: pusher "chasing" disk around a circular path.

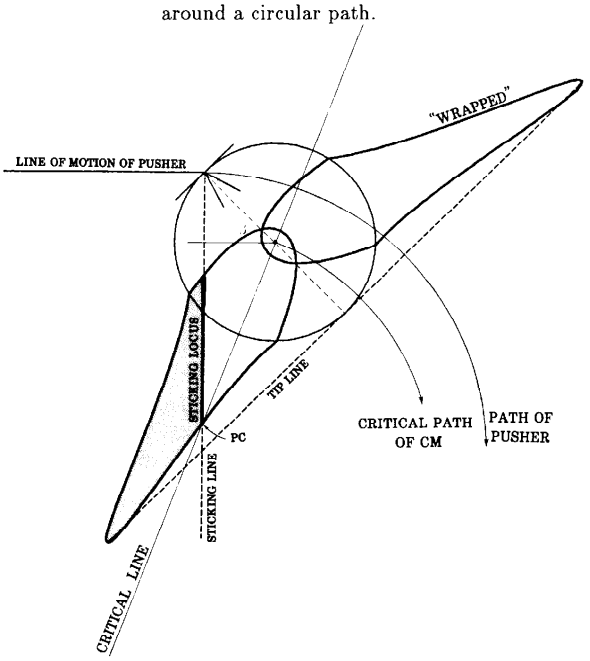


**Figure 4-3:** COR sketch for critical case, and solution for location of *PC*.

### 4.3. Critical Radius vs. Collision Parameter

For every value of $\beta$, (the collision parameter), we compute the distance from the pusher's line of motion to the lower endpoint of the sticking locus. This defines a critical radius $r^*(\beta)$. For each collision parameter $\beta$, $r^*(\beta)$ is the radius of the tightest circle that the pusher can describe with the guarantee that the disk will be pushed into the circle. In figure 4-4, $a / r^*(\beta)$ is plotted as a function of collision parameter $\beta$ for each of several values of $\mu_c$.

The inverse of the function $r^*(\beta)$ will be denoted $\beta^*(r)$, representing the smallest value of $\beta$ for which a pusher motion of radius $r$ still results in guaranteed localization. In terms of the pusher's distance from the top edge of the disk, $d$, (figure 4-3), we can use the relationship

$$a\,(1-\sin\beta) = d \tag{2}$$

to define the *critical distance from grazing* $d^*(r)$ as a function of $r$. $d^*(r)$ is the largest distance of the pusher from the top edge of the disk for which a pusher motion of radius $r$ still results in guaranteed localization.

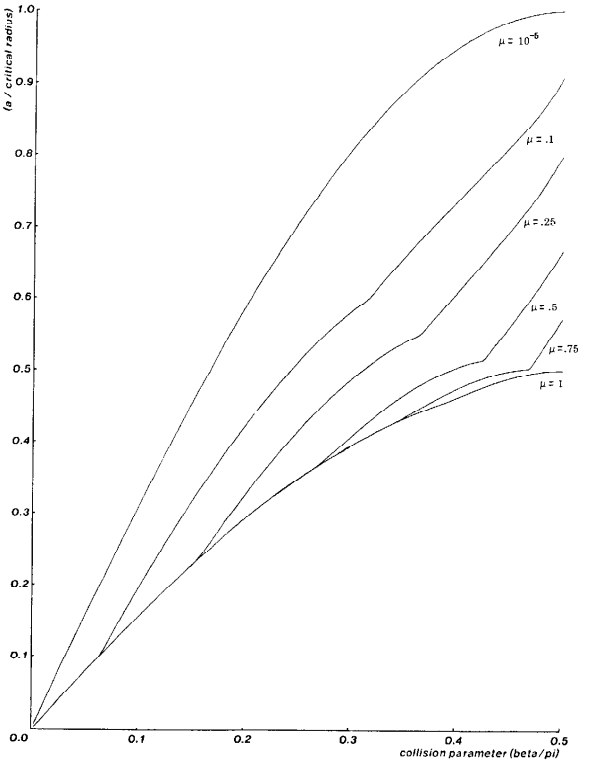


**Figure 4-4:** Inverse of the radius of the critical circle $r^*(\beta)$ as a function of collision parameter $\beta/\pi$.

### 4.4. Limiting Radius for Localization

If there is a limiting radius $b_\infty$ of the spiral motion below which localization cannot be guaranteed, then as the spiral approaches radius $b_\infty$ the motion must become circular. $\Delta b \to 0$ as $b_\infty$ is approached, so collisions become grazing collisions, and we have the distance from grazing $d \to 0$. (In terms of the collision parameter $\beta$, we have $\beta \to \pi/2$.) If the disk is not to be bumped out of the spiral, we must have $b_\infty = r^*(\beta{=}\pi/2)$. $b_\infty$ can be shown analytically to be

$$b_\infty = a\,(\mu_c + 1) \quad \text{for } \mu_c \le 1 \tag{3}$$

$$b_\infty = 2\,a \quad \text{for } \mu_c \ge 1$$

We see that only if $\mu_c = 0$ can a disk be localized completely, i.e. localized to within a circle the same radius as that of the disk. Otherwise the tightest circle within which the disk can be localized is given by equation 3.

### 4.5. Computing the Fastest Guaranteed Spiral

Let $b_n$ be the radius of the $n^{th}$ revolution of the pusher, so that we have initially radius $b_1$, and $b_\infty$ is the limiting radius as $n \to \infty$. We define recursively

$$b_n = b_{n-1} - d^*(b_n) \tag{4}$$

The difference between the radii of consecutive turns of the spiral $n-1$ and $n$, is $\Delta b = d^*(b_n)$. Equation 4 thus enforces the condition that on the $n^{th}$ revolution, the value of $d$ is exactly the critical value for circular pushing motion of radius $b_n$.

Figure 4-5 shows the deviation of spiral radius $b_n$ above $b_\infty$, vs. number of turns $n$, on logarithmic and on linear scales. We start (arbitrarily) with $b_1 = 100\,a$. The spiral radius was computed numerically for $\mu_c = .25$, using the results for $\beta^*(r)$ shown in figure 4-4, and equation 4.

Figure 4-5 shows that when the spiral radius is large compared to the disk radius $a$ (which is taken to be 1 in the figure), we can reduce the radius of the spiral by almost $a$ with each revolution. As the limiting radius is approached, the spiral reduces its radius more and more slowly, approaching the limiting radius $b_\infty$ as about $n^{-1.6}$, where $n$ is the number of revolutions.

Figure 4-5 demonstrates the best performance that the "herding" strategy can achieve.

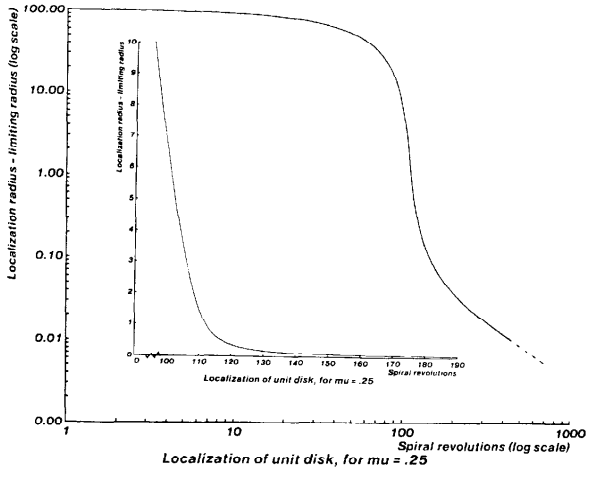


**Figure 4-5:** Deviation of spiral radius from ultimate localization radius, vs. number of spiral revolutions completed.

## 5. Conclusion

We have shown how bounds can be placed on the possible instantaneous motions of a sliding object being pushed by another object, in the presence of unknown frictional forces between object and table, and between object and pusher. These bounds provide the basis for planning manipulation of sliding objects with or without sensors. As an example a sensorless strategy for localizing a disk was developed and optimized. We believe that the motion of a sliding object is now sufficiently well understood that reliable robot strategies taking advantage of sliding motion can be designed and verified.

## References


**1.** Brost, Randy. Automatic Grasp Planning in the Presence of Uncertainty. Proceedings, IEEE Int'l Conf. on Robotics and Automation, April, 1986.

**2.** Mani, Murali and Wilson, W. R. D. A Programmable Orienting System for Flat Parts. Proceedings, NAMRII XIII, 1985.

**3.** Mason, Matthew T. and Salisbury, J. K.. *Robot Hands and the Mechanics of Manipulation*. The MIT Press, 1985.

**4.** Mason, Matthew T. On the Scope of Quasi-static Pushing. Proceedings, 3rd Int'l Symp. on Robotics Research, October, 1985.

**5.** Pingle, K., Paul, R., Bolles, R. Programmable Assembly, three short examples. Film, Stanford AI Lab, 1974.

**6.** Peshkin, M. A. and Sanderson, A. C. The Motion of a Pushed, Sliding Object (Part 1: Sliding Friction). CMU-RI-TR-85-18, Robotics Institute, Carnegie-Mellon University, 1985.

**7.** Peshkin, M. A. and Sanderson, A. C. The Motion of a Pushed, Sliding Object (Part 2: Contact Friction). CMU-RI-TR-86-7, Robotics Institute, Carnegie-Mellon University, 1986.